Original papers

Towards the applicability of biometric wood log traceability using digital log end images ☆

CrossMark

R. Schraml [a,*], J. Charwat-Pessler [b,*], A. Petutschnigg [b], A. Uhl [a]

[a] University of Salzburg, Jakob Haringer Str. 2, 5020 Salzburg, Austria
[b] University of Applied Sciences Salzburg, Markt 136a, 5431 Kuchl, Austria

ARTICLE INFO

ABSTRACT

Log traceability in the timber based industries is a basic requirement to fulfil economical, social and legal requirements. This work introduces biometric log recognition using digital log end images and explores the robustness to a set of log end cross-section (CS) variations. In order to investigate longitudinal and surface CS variations three tree logs were sliced and captured in different sessions. A texture feature-based technique well known from fingerprint recognition is adopted to compute and match biometric templates of CS images captured from log ends. In the experimental evaluation insights and constraints on the general applicability and robustness of log end biometrics to identify logs in an industrial application are presented. Results for different identification performance scenarios indicate that the matching procedure which is based on annual ring pattern and shape information is very robust to log length cutting using different cutting tools. The findings of this study are a further step towards the development of a biometric log recognition system.

© 2015 The Authors. Published by Elsevier B.V. This is an open access article under the CC BY license (http://creativecommons.org/licenses/by/4.0/).

1. Introduction

Many efforts had been made in the past in order to investigate illegal logging, its associated causes and how to prevent from illegal logging in future. Besides corruption on different governmental authority levels and land reclamation for mining, plantations or agriculture, illegal logging is known to be one of the main driving forces promoting deforestation (Richards et al., 2003; Smith et al., 2003; Kuemmerle et al., 2009). Deforestation is a phenomenon comprising timber harvesting, timber trade and disposal occurring around the world and affects biodiversity, hydrological cycles and contributes considerably soil erosion.

These problems were officially addressed at the UN Conference on Environment and Development (UNICED) held in Rio de Janeiro in 1992 and concluded in a document called Agenda 21. This document provides voluntary commitments on sustainable forest management and development and offers a basis for non-governmental, independent forest certification (United Nations, 1992). According to a report supported by the World Bank in 2003, illegal logging is still considered a major threat to the environment (Dykstra et al., 2003). Efforts in fighting illegal logging on the EU level led to the Forest Law Enforcement Governance and Trade Action Plan (FLEGT) defined in 2003 and the EU Timber Regulation (EUTR) prohibiting the trade of illegally harvested timber and wood products derived therefrom. This regulation, initially proposed by the Commission in 2008, is legally binding on all EU member states, each being responsible for national implementation, and has come into force since March 2013. This regulation claims traceability of timber and timber products throughout the supply chain providing information on operators, traders and, if possible, of retailers (EuropeanParliament, 2010).

Traceability of timber and wood products is generally expected to restrict illegal logging and is supposed to benefit companies and consumers (Tzoulis and Andreopoulou, 2013). In fact empirical information on quantities, and links to internationally traded wood are indispensable in order to assess causal relationships for illegal logging and to take effective steps preventing deforestation in future (Kastner et al., 2011). A contemporary managed database in conjunction with log labelling would certainly provide this information and serves as basis to impede illegal logging, fraud and misuse in future.

A wide variety of log traceability systems have been applied in order to identify and track logs in the past. Each method so far has shown limitations due to costs, practical implementation or weather conditions. The applications range from punching, coloring or barcoding log ends to more recently developed techniques as DNA fingerprinting and usage of RFID transponders (Tzoulis and Andreopoulou, 2013).

Another approach is to track logs using biometric log characteristics. Investigations on the hypothesis that logs are separate entities on the basis of biometric log characteristics were presented in the works of Chiorescu and Grönlund (2003, 2004), Flodin et al. (2007, 2008a,b), which highlight the potential of biometric log recognition. The approaches presented in Chiorescu and Grönlund (2003, 2004) and Flodin et al. (2008a) utilized 2D and 3D scanners to extract geometric wood properties for tracking logs within the sawmill environment. The utilized capturing devices are however, not applicable at forest site. Furthermore, Flodin et al. (2007, 2008b) showed that knot positions as biometric features are suited to enable traceability between logs and the cut boards, reaching a recognition rate of 95%. On account of the fact that timber offers characteristics on log end faces in terms of annual rings, pith position, shape and dimension it is assumed that cross-section images of log ends can be used as biometric characteristic for log identification. Approaches for pith estimation and annual ring measurements in images of rough log ends were presented in Norell and Borgefors (2008), Schraml and Uhl (2013), Marjanen et al. (2008) and Norell (2009), respectively. Images containing a cross-section (CS) of a wood log are denoted as cross-section images (CS-Images) throughout this work.

A first work on log biometrics using CS-Images (log end biometrics) was presented in Barrett (2008) as an effort to curb poaching of trees. In the experimental evaluation digital images of tree stumps and the corresponding log ends are utilized, both showing up strong saw kerf patterns. Results show that the combination of log end shape and saw cut pattern information, represented by Zernike polynomials, achieves a high accuracy for log to stump recognition. In Schraml et al. (2014) temporal and longitudinal annual ring pattern variations were investigated based on time-delay captured CS-Images of 35 slices from a single log.

By using CS-Images from 150 different logs (Schraml et al., 2015a) showed that fingerprint based and iris-recognition based approaches are suited to achieve 100% identification accuracy. It turned out that, in addition to annual ring pattern information shape information is required to achieve this accuracy. Based on this observation in Schraml et al. (2015b) the discriminative power for a set of geometric log end features was validated.

In this study we elaborate the robustness of log end biometrics to practical issues of an industrial application. Different CS-Images of the same log end show up strong variations. For example, CS-Image capturing and weather conditions may lead to strong variations: e.g. varying image quality caused by motion blur or different lighting conditions and snow or dirt which covers parts of the CS. These variations are not considered in this work. Furthermore, industrial log processing causes specific types of CS variations. For this work we focus on longitudinal and surface variations of cross-sections (CSs). Longitudinal variations result from log end cutting and surface variations arise when different cutting tools are utilized for the first cut, in the forest, and the clearance cut, by further processing company (e.g. chain-saw and circular-saw).

The experimental evaluation is based on a testset which consists of 99 CS-Slices from three different tree logs. In addition to the 35 CS-Slices from the single log used in Schraml et al. (2014), 64 CS-Slices from further two logs are utilized. By assessing two objectives this work contributes to the ongoing research on log end biometrics.

The first objective is to investigate the verification performance with respect to the impact of surface and longitudinal variations on the intraclass variability and the separability between the intra- and interclass score distributions. In this context we also assess whether the CS surface has an impact on the longitudinal variations of each log.

The second objective is to investigate the identification performance. Initially, the basic impact of surface and longitudinal variations on the identification performance is assessed. Second, different real world-like identification scenarios are evaluated.

First, Section 2 introduces the computation and matching of biometric templates from CS-Images. The experimental setup is presented in Section 2.4 followed by the results in Section 3. Section 4 concludes this work and in Section 5 directions for future work are outlined.

2. Materials and methods

By superficially comparing the patterns of human fingerprints to annual ring patterns of wood log ends, one finds a close resemblance. Human fingerprint recognition is well-investigated and there exist mainly three groups of approaches: Minutiae-based, Correlation-based and Feature-based approaches (Maltoni et al., 2009). Apart from the presence of the pith as detectable feature, CS patterns do not exhibit further constant features like minutia's in fingerprints. Hence, minutiae-based approaches are not qualified for log CSs.

Basically, the scheme of a biometric recognition system is set up on five components: Data acquisition, Preprocessing, Feature Extraction, Template Generation and Template Matching. In case of log end biometrics, data acquisition is the capturing of digital CS-Images of log ends. For preprocessing the CS in the CS-Image is separated from the background, aligned and subsequently the CS is enhanced. Due to the ability of feature-based methods to capture information of the fingerprint ridge pattern they can be extended to work with CS patterns. We have adopted the texture feature-based FingerCode approach by Jain et al. (2000, 2001) to extract features from CS-Images. The extracted features of a CS-Image are stored as feature vector into the biometric template which we denote as cross-section code (CS-Code). The CS-Code of a CS-Image is composed by a set of feature vectors which are computed for differently rotated versions of the CS-Image.

Finally, template matching is the task of verification or identification of an individual or subject. In case of wood logs, identification is required. For this purpose, the individual/subject must be enrolled in the biometric system. In Fig. 1 exemplary enrolment and identification schemes are depicted. Enrolment could be done during the harvesting procedure in the forest. A digital camera mounted on a
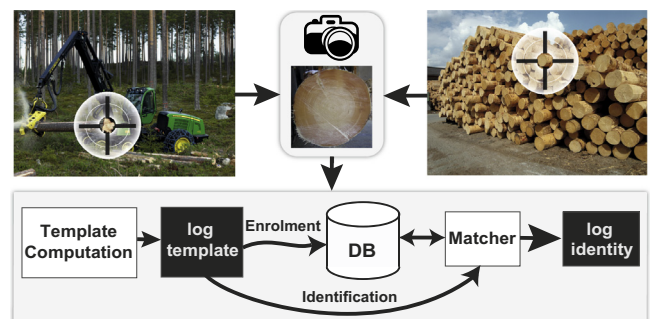

Fig. 1. Exemplary enrolment and identification schemes for a biometric log recognition system. The enrolment can be done in the forest using a digital camera mounted on a harvester.

harvester (e.g. Mattila and Viittanen, 1999) could be utilized to capture one end of each fresh cut log. Subsequently, the first four steps of the biometric system chain are completed and the computed log template (CS-Code) is stored in a database. Additionally, informational meta data can be assigned to each log template: On the one hand the harvester operator can assign visually observed information and the ownership of each log. Furthermore, geometric measurements of the harvester head and the geospatial position of the log origin can be appended. On the other hand automated CS analysis can be performed to estimate properties related to the quality of each log, e.g. annual ring counting to estimate the strength or detection of quality related wood properties like reaction wood.

Now identification of each log can be performed at each stage of the log processing chain. CS-Images for identification in the sawmill could be captured at the sorting station, at the sawmill yard or at any conveyor belt equipped with a capturing device. Subsequently, the CS-Image is processed by the biometric system and a log template is computed which is matched to all log templates in the database. If the matching score (MS) exceeds a certain system threshold the best match specifies the identity of the log. Furthermore, additional meta data can be retrieved or appended from/to the log record in the database. Templates of logs which were further processed and are no longer required should be removed from the database. May the log template is passed to another biometric system which enables board tracking (biometric approach: Pahlberg et al., 2015) and connects each board to the log template from which it descends. However, for chain of custody certification specific log template information has to be linked or passed through to the final product.

In the next three sections a detailed introduction on preprocessing (Section 2.1), CS-Code computation (Section 2.2) and three matching procedures (Section 2.3) between two CS-Codes is given. Finally, in the last Section 2.4 basics for the experimental evaluation are introduced.

2.1. Cross-section registration & enhancement

Due to the cutting pattern annual ring enhancement is a crucial task for any subsequent feature extraction procedure. As opposed to human fingerprints, the frequency of the annual ring pattern is strongly varying. Similar as in our previous works (Schraml et al., 2014, 2015a) enhancement is based on the fingerprint enhancement approach presented by Hong et al. (1998). In Schraml et al. (2015a) we showed that a slight variation of the procedure utilized in Schraml et al. (2014) further improves the biometric system performance and is thus also used in this work.

Preliminary to enhancement the CS in a CS-Image has to be registered. For registration, the CS border and pith position have to be determined (e.g. Schraml and Uhl, 2014, 2013; Norell and Borgefors, 2008). Subsequently, the CS-Image is rotated around the pith position, cropped to the CS bounding box and finally scaled to 512 pixels in width (see Fig. 2). Rotation can be performed to generate rotated versions of each CS-Image or to align the CS to a unique position (e.g. according to the center of mass).

For enhancement three consecutive stages are performed: Local orientation estimation, local frequency estimation and local adaptive filtering. First, the CS is subdivided in half-overlapping blocks (e.g. 32×32 pixels). Half-overlapping blocks are used to reduce boundary effects caused by local filtering. For each block principal component analysis of the local Fourier spectrum is performed to determine its local orientation (see Schraml and Uhl, 2013). Commonly, CSs are disturbed, due to cutting, which leads to faulty orientation estimates. For this purpose the local orientation is compared to the direction given by the block-centre to pith position vector (block-pith vector). If the angular distance between the local orientation estimate and the block-pith vector orientation exceeds a certain threshold (t) the local orientation estimate is
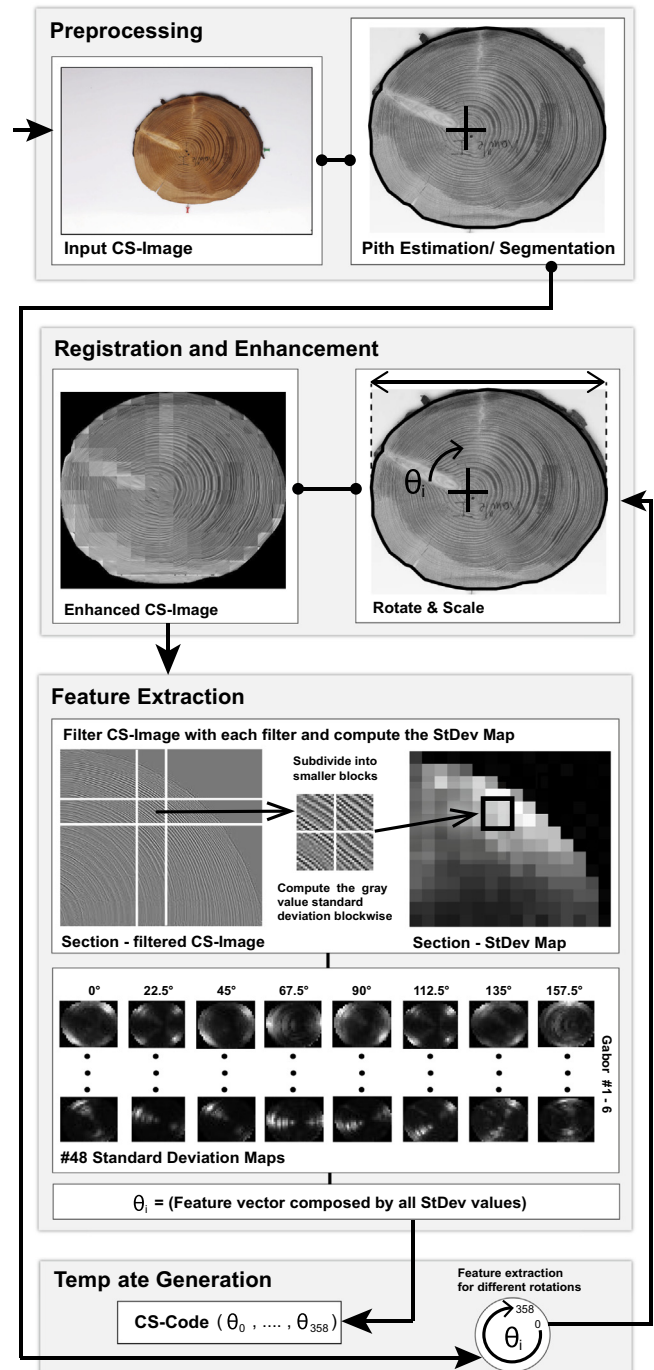

Fig. 2. Log template/CS-Code computation illustration.

considered being wrong. For each block t is defined by $t = \lambda * \log(\text{pith distance})$, where λ is an arbitrary value and the pith distance is the length of the block-pith vector. Thus, the threshold increases with an increasing pith distance which takes into account that annual rings close to pith are more circular. Local orientation estimates which exceed this threshold are replaced by the block-pith vector orientation.

Next, for each block and its local orientation the dominant frequency is determined. For this purpose, the local Fourier spectrum of each block is subdivided into sub-bands and sectors. For each sector and each particular sub-band the integral of the contained magnitudes is computed. The sector sub-band which shows the maximum sum of magnitudes represents the dominating frequency. If the local orientation which corresponds to this sector

sub-band is not the same as the previously determined block orientation it is neglected. In this case the local frequency is interpolated using a Gaussian.

Finally, in the filtering stage the Fourier spectrum of each block is filtered with a Log-Gabor (introduced by Knutsson and Granlund, 1983) which is tuned to the local orientation and frequency of the corresponding block. Similar as in Schraml et al. (2014, 2015a) a bandwidth of three times the variance of the Fourier spectrum and a spread value of blocksize/4 are utilized. The filtered Fourier spectra are inverse Fourier transformed and the results are subsequently used as new block values. An exemplary result of the registration & enhancement procedure is depicted in Fig. 2.

2.2. Cross-section code computation

The CS-Code computation is based on the FingerCode approach proposed in Jain et al. (2000, 2001). This technique utilizes a Gabor-based descriptor which extracts local ridge orientations of a fingerprint. Because of the constant ridge frequencies in human fingerprints a single Gabor filter and its rotated versions are sufficient. The frequencies of annual ring patterns are strongly varying and thus different Gabor filters are required to capture additional information from the annual ring frequencies in different orientations. For a CS-Image width of 512 pixels six different Gabor filters are suggested. For each Gabor filter eight rotated versions are created. Consequently, the Gabor filterbank consists of 48 filters:

$$G(\lambda, \theta, \sigma, \gamma) = G(\lambda, \sigma)$$
$$= ((1.5, 1), (2.5, 2), (3.5, 3), (4.5, 3), (5.5, 3), (6.5, 3)),$$
$$\theta = \{0, 22.5, \ldots, 135, 157.5\}, \gamma = 0.7$$

Feature extraction (Fig. 2) is performed in three stages. In the first stage the enhanced CS-Image is filtered with each filter in the filterbank. Each filtered image is subdivided into blocks (8×8 pixels). For all blocks of each filtered image the gray value standard deviations are computed and stored into a matrix, which is denoted as Standard Deviation (StDev) map. Altogether 48 StDev maps are computed and are stored as one-dimensional feature vector (θ) in the CS-Code. Blocks which are not within the CS border are assigned a marker value which is relevant for CS-Code matching. Furthermore, two CS-Images of the same log end or CS-Slice can be rotated differently. Rotational differences are compensated by computing feature vectors for rotated versions of the input CS-Image in the expected misalignment range. Although the misalignment range in this work is much smaller, feature vectors for 180 rotations in two degree steps are computed and used for matching. Hence, it can be evaluated if there exist rotated versions of two CS-Slice images from different tree logs which are incidentally similar to each other. All feature vectors computed for different rotations ($\theta_0, \theta_2, \ldots, \theta_{356}, \theta_{358}$) compose the CS-Code of a CS-Image (see Template Generation in Fig. 2).

2.3. Cross-section code matching

In contrast to fingerprints where the shapes are commonly not utilized, the CS shape is obviously a biometric feature itself. By investigating three different matching procedures the discriminative power of the annual ring pattern, the shape and a fusion of both is evaluated.

The first procedure which just considers annual ring pattern information is denoted as annual ring pattern MS (MS_{AP}) and is defined as the minimum MS between the feature vectors of both CS-Codes:

$$MS_{AP}(\text{CS-Code}_1, \text{CS-Code}_2) = \min MS(\theta_i, \theta_j)$$
$$\text{where} \quad \theta_i \in \text{CS-Code}_1(\theta_0, \ldots, \theta_{358}),$$
$$\theta_j \in \text{CS-Code}_2(\theta_0, \ldots, \theta_{358}) \tag{1}$$

Due to interpolation in the registration procedure (rotation and scaling) the best MS is achieved when comparing all feature vectors of both CS-Codes. The MS between two feature vectors of two CS-Codes is computed by:

$$MS(\theta_i, \theta_j) = \frac{1}{M} \sum_{k=0}^{n} D(\theta_i(k), \theta_j(k)) \tag{2}$$

where θ_i, θ_j are two feature vectors of the CS-Codes which are compared, k specifies the index of the feature value in both vectors, n is the max. number of feature values and M is a normalization factor. The utilized distance function is given by:

$$D = \begin{cases} |\theta_i(k) - \theta_j(k)| & \text{if } k \in MCS_i \cap MCS_j \\ 0 & \text{otherwise} \end{cases} \tag{3}$$

As noted in Section 2.2, background feature values are specified by a certain marker. Hence, we define MCS_i and MCS_j as the corresponding masks of the feature vectors which allow to differentiate between background and CS. Just feature vector value pairs which are in the intersection of both CSs are utilized for computing MS_{AP} and the score is normalized by the amount of the considered feature value pairs: $M = |MCS_1 \cap MCS_2|$.

The second procedure (MS_F) is a measure describing the similarity of the shapes of two CSs. MS_F is defined as the minimum False Negative Rate (F) between the masks of the feature vectors of both CS-Codes:

$$MS_F(\text{CS-Code}_1, \text{CS-Code}_2) = \min F(MCS_i, MCS_j) \tag{4}$$

The False Negative Rate (F) between two different masks (MCS_i, MCS_j) is computed by:

$$F = \frac{MCS_i \Delta MCS_j}{\min(|MCS_i|, |MCS_j|)} \tag{5}$$

Finally, the last procedure ($MS_{AP,F}$) is based on score level fusion (Jain et al., 2011, p. 225) of MS_{AP} and MS_F. For score level fusion both scores are combined using different scaling factors (see Eq. (6)). The scaling factors ($\sigma_{AP}, \sigma_{MS_F}$) are determined from their score distributions to ensure that both contribute equally to the combined MS.

$$MS_{AP,F} = MS_{AP} \cdot \sigma_{AP} + MS_F \cdot \sigma_F \tag{6}$$

2.4. Experimental setup

2.4.1. Testset

The experimental evaluation is based on cross-section slices (CS-Slices) from three different European spruce logs (Log 1 – L1, Log 2 – L2, Log 3 – L3). For L1 and L2, a section of 40 centimetres was cut into 16 CS-Slices. The CS-Slices were cut with a bandsaw and the thickness of each CS-Slice is approximately 2.5 centimetres. The sections of L1 and L2 were showing a diameter of around 230 mm and 290 mm respectively.
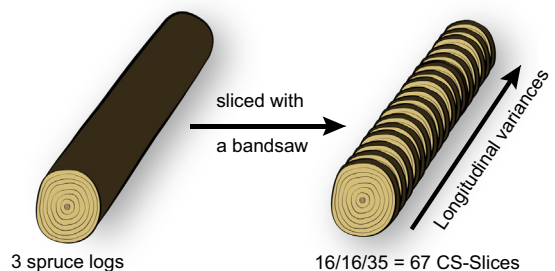

Fig. 3. In total 67 CS-Slices from three different logs are cut-off.

Table 1
Testset overview.

3 Logs	# CS-Slices	# CS-Images	Illustration
Log 1 – L1	16	2 (Rough & Sanded)	Fig. 4a
Log 2 – L2	16	2 (Rough & Sanded)	Fig. 4b
Log 3 – L3	35	4 (Time delay)	Fig. 5

Subsequently, just one surface of each CS-Slice was captured two times (Nikon D90). The first CS-Image was taken from the fresh cut CS-Slices. For the second CS-Image, the surfaces of the CS-Slices were polished using a sandpaper (P 150). In the first row of Fig. 4 the two captured CS-Images of one CS-Slice from L1 and L2 are depicted.

To increase the number of interclass scores, a third log (L3) with a total of 35 CS-Slices with 2 cm spacing is utilized. Each CS-Slice was captured with four different time delays (Fig. 5). For a detailed dataset description we refer to Schraml et al. (2014) (see Table 1). For all CS-Images in the testset the pith position and the border of the were determined manually and are utilized for CS registration and defining the CS-Masks in the experiments. The CS-Images in Fig. 4 illustrate the preprocessing steps for the CS-Images of the CS-Slices L1 #2 and L2 #10. In the first row the original images are depicted. The second and third row show the registered and enhanced versions of the CS-Images, respectively. The four time-delay captured CS-Images of CS-Slice L3 #10 are depicted in Fig. 5.

2.4.2. Evaluation background

Before presenting the results, relevant basics for the experimental evaluation are introduced. First, a short introduction on biometric performance evaluation is presented. Subsequently, three types of wood log CS variations are defined and the construction of the intra- and interclass score distributions (SDs) used in the evaluation is described.

Biometric performance evaluation. Commonly, a biometric system operates either in verification or identification mode and the term recognition is used universally.

For verification the system compares a query template to just one template of the database (1:1 comparison). This template is specified by the claimed identity of the query template. The system accepts or rejects the claimed identity of the individual/object. For identification a query template is compared to all templates in the database (1:N comparison) and if the best match exceeds a certain system threshold it specifies the identity of the query template.

Generally, a biometric system is assessed based on the errors it produces (Maltoni et al., 2009). Two major verification system errors (False Match Rate (FMR) and False Non Match Rate (FNMR)) result from the calculation of the intra- and interclass SDs which are commonly denoted as genuine and impostor SD, respectively. The intraclass SD contains all MSs computed between a set of templates of the same individual. The interclass SD contains the MSs between templates of different individuals. Consequently, the FMR includes all MSs between different individuals which are incorrectly accepted by the system. On the other hand the FNMR gives the proportion of MSs which were rejected although the score is computed between templates of the same individual. For verification performance evaluation the equal error rate (EER) is a general benchmark. The EER is defined as the error where FMR and FNMR are equal.

Fig. 5. Temporal variations: L3 CS-Slice #34, sessions 1–4 (Schraml et al., 2014).

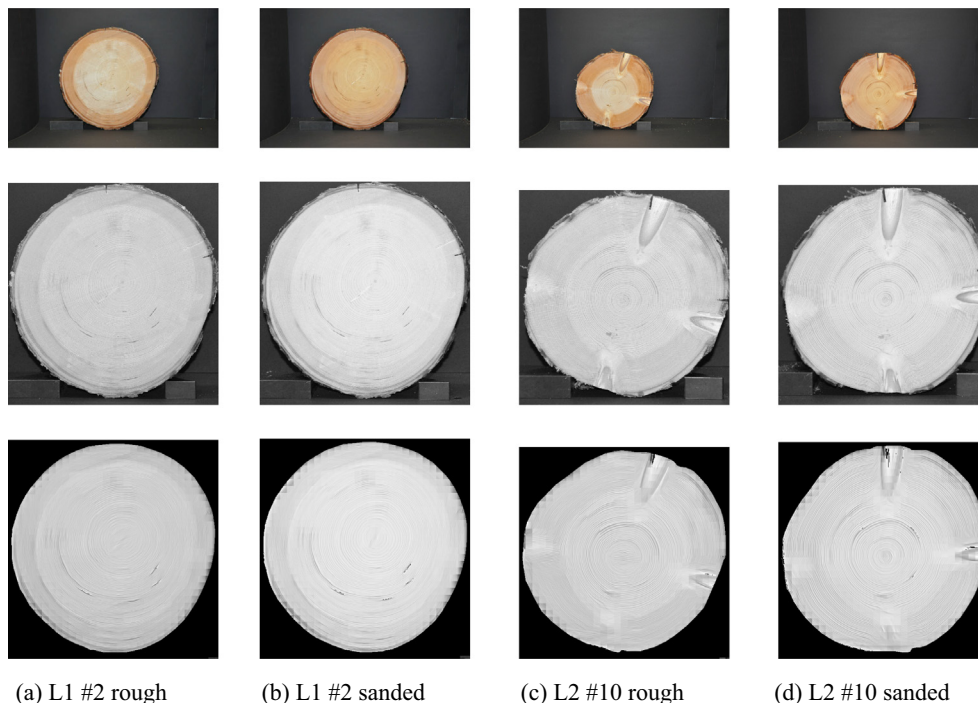| (a) L1 #2 rough	(b) L1 #2 sanded	(c) L2 #10 rough	(d) L2 #10 sanded

Fig. 4. Testset examples: Slices #2 and #10 from L1 and L2, respectively. The CS-Images in the first row depict the original CS-Images and in row two and three the registered and enhanced CS-Images used for CS-Code computation are illustrated.

The identification performance is evaluated by matching a set of probe templates to all templates enrolled in the database (Jain et al., 2007). We refer to closed-set identification where it is assumed that all individuals/objects of the probe templates are enrolled in the system. The MSs between each probe template and all database templates are ordered according to the MS. The ordered MSs of each probe template are used to compute the probability that the correct template is ranked within the top k-ranked MSs. The probabilities for each rank are illustrated in a curve which is denoted as Cumulative Match Characteristic (CMC).

Wood log cross-section variability. Two basic requirements for biometric recognition are uniqueness and permanence of the utilized biometric characteristic. Uniqueness expresses that the biometric characteristic and the computed templates of different individuals are strongly varying and permanence is the requirement that they do not change over time. Related to those requirements there are two basic issues which a biometric system must handle: Intraclass variability and Interclass similarity which contribute to the F NMR and FMR, respectively. Interclass similarity is the problem that different individuals may show up similar biometric characteristics. Intraclass variability is an issue due to internal and external caused variations between a set of templates of the same individual. External variations occur due to irregularities in the template generation procedure, e.g. different sensors or capturing environments. Furthermore, the visual appearance of the biometric characteristic is affected or modified by external influences, e.g. the saw cut pattern. Internal variations are eventually caused by an intrinsic modification or change of the biometric characteristic itself, e.g. temporal variations caused by the ageing process. In case of human biometrics, it is attempted to overcome external and internal changes/modifications by updating the stored templates in the database.

In case of wood logs, several external and internal caused variations/modifications of CSs of a single log have an impact on the intraclass variability. So far, three different variation types emerged from our research:

- **Temporal variations** correspond to the issue of ageing in human biometrics. In case of wood log ends, the visual appearance of a CS changes rapidly. Due to the rapidly changing moisture content at the log end faces and the sun exposure the CS shows up discolourations or deformations (e.g. cracks). In Fig. 5 four time-delay captured CS-Images of a CS-Slice from L3 illustrate temporal variations.
- **Longitudinal variations** are caused by the changing CS pattern along the longitudinal axis of a single tree log. Consequently, they address the issue of length-cutting a log in the sawmill. Cut-off lines are utilized in many sawmills for different reasons. For example, clean log end faces (no stones and sand) are beneficial to protect the cutting blades and to aid the log quality assessment. On the other hand, log end cutting leads to a loss of material and is not tolerable in certain fields of the sawmill industry. An illustration for longitudinal variations of the CSs from a single log is presented in Fig. 6.
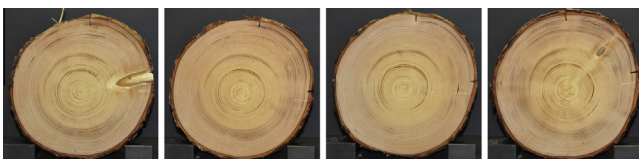

Fig. 6. Longitudinal variations: L2 CS-Slices #1, 4, 8, 16.

Table 2
Intraclass SD groups.

CS variation	SD group details
Longitudinal SD	L1 & L2: MSs between the rough or sanded CS-Images of their CS-Slices
Surface SD	L1 & L2: MSs between the rough and sanded CS-Image of each CS-Slice

- **Surface variations** result from differently finished or cut surfaces of a particular CS. In this work surface variations between saw cut CS surfaces and the sanded CS surface counterparts are assessed (see Fig. 4). Another scenario which is closely related to industrial biometric log recognition involves CS surface variations caused by different cutting tools (e.g. chain-, band- or circular saw). Probably the first cut in the forest and the cleansing cut in the sawmill are performed with different devices. This results in a mixture of longitudinal and surface variations.

For the testset CS-Images of the CS-Slices from L1, L2 and L3 we tried to avoid external variations which are caused by the capturing procedure.

Intra-/interclass score distributions (SDs). For the evaluation, the MSs between all CS-Images of L1, L2 and L3 are computed using the proposed matching procedures. The intra-/interclass SDs for a single matching procedure are constructed by grouping the MSs into the respective SD. Hence, the interclass SD contains all MSs computed between the CS-Images of L1, L2 and L3. The intraclass SD is built up on the MSs between CS-Images of the same log and is further subdivided into two SD groups corresponding to the variation type (see Table 2). Temporal variations which are represented by the MSs between the four time-delay captured CS-Images of each CS-Slice from L3 were investigated in Schraml et al. (2014) and are not treated in this work. The longitudinal SD shows the similarity between CS-Images which were captured at different longitudinal positions of the same log. In this work we consider the longitudinal variations of L1 and L2. For this purpose, the longitudinal SD is built up on the MSs between the CS-Images of rough or sanded CS-Slices from L1 and L2. The surface SD includes all MSs between the saw cut CS surfaces and the sanded CS surface counterparts of each CS-Slice from L1 and L2.

3. Results and discussion

The results of the experiments are subdivided into two sections. Section 3.1 presents investigations on the separability between the intra- and interclass SD. For this purpose, the verification performance of the biometric system for different matching procedures is assessed and the EERs are considered.

Because of the manifold structure of the intraclass SD an exhaustive analysis of the longitudinal and surface SD group is presented in Section 3.2. Based on the results, fundamental conclusions on the intraclass variability and the impact on the separability between the intra- and interclass SD are drawn. Finally, Section 3.3 treats the identification performance for different real world scenarios.

3.1. Intra-/interclass SD separability

In Fig. 7 the intra-/interclass SDs for all three matching procedures are illustrated. Most important, the charts show that the best EER is achieved by $MS_{AP,F}$ which uses both annual ring pattern and shape information. Furthermore, the EERs for MS_{AP} and MS_F illustrate that for the considered three logs shape information is less discriminative compared to annual ring pattern information. In addition, Table 3 depicts EERs for different intra-/interclass SD
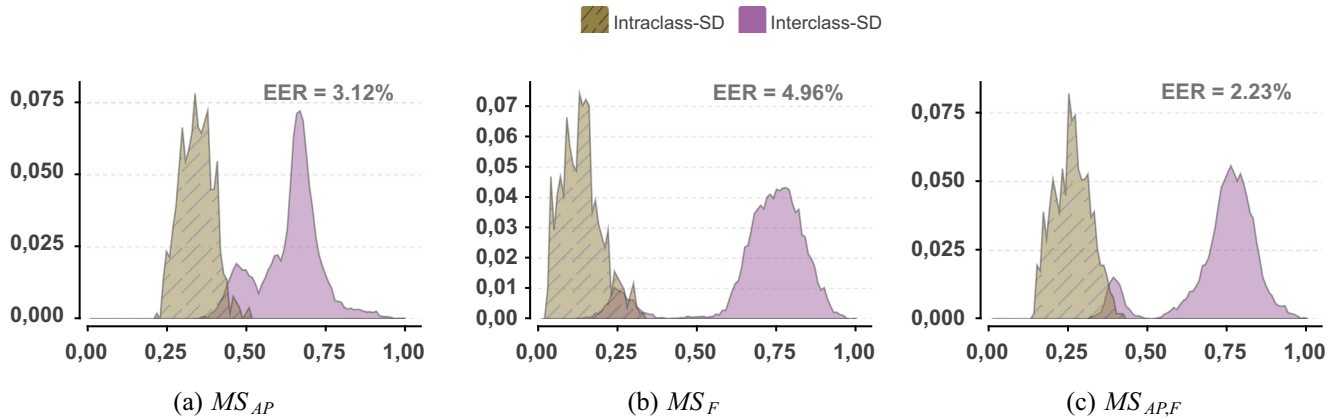
Fig. 7. Intra-/interclass score distributions (SD) for different matching procedures. [*X*-Axis: Matching Score, *Y*-Axis: Probability].

Table 3
EERs [%] for all matching procedures and different subsets of L1, L2, L3.

Logs	MS_{AP}	MS_F	$MS_{AP,F}$	
L1–L2	5.6	12.79	12.85	6.21
L1–L3	0.11	0.48	0.0	0.0
L2–L3	3.57	5.07	0.0	0.0
L1–L2–L3	3.12	5.38	4.96	2.23

subsets of the three logs. The results for MS_F and L1–L2 illustrate that L1 and L2 have a similar shape which causes a bad EER of 12.85%. In case of L1–L3 and L2–L3 the shapes are very distinctive which leads to a zero EER. Considering MS_{AP} and the annual ring pattern distinctiveness the results show that the pattern of L1 is more similar to L3 than the pattern of L2 to L3. It can be concluded that for different tree logs the discriminative power of the annual ring pattern and the shape varies significantly. Consequently, the robustness of log end biometrics benefits from using shape and annual ring pattern information together.

Generally, an EER of ∼2% for $MS_{AP,F}$ is astonishing because the intraclass SD includes all longitudinal MSs for all slice distances. Our experiments in Schraml et al. (2014) showed that the similarity between different CS-Slices of a log deteriorates with an increasing distance between the considered CS-Slices. A detailed analysis of the intraclass SD groups (Longitudinal and Surface SD) allows to gather further insights.

3.2. Intraclass SD analysis

In this section the longitudinal and surface SD groups of which the intraclass SD is build up are assessed in detail.

3.2.1. Longitudinal SD

The longitudinal SD contains the MSs between the rough or sanded CS-Images of the CS-Slices from L1 and L2. Four subsets of the longitudinal SD are assessed in detail: Rough & Sanded longitudinal MSs of L1 and L2. The MSs of each subset are grouped according to the neighbourhood distance of the compared CS-Slices. In case of 16 CS-Slices for each log the distance between two CS-Slices ranges from 1 to 15 which leads to 15 slice distance groups (SDGs). For example, SDG 1 contains all MSs of each CS-Slice to the adjacent neighboured CS-Slices.

In Fig. 8 the mean values of each subset and SDG for all matching procedures are depicted. For MS_{AP} it is expected that the longitudinal MSs increase the higher the slice distance between two CS-Slices is. An increase or change of the MSs for higher slice distances can also be expected for MS_F and $MS_{AP,F}$. In Schraml et al. (2014) our experiments based on CS-Slices from L3 confirmed this expectation.

Let's consider MS_{AP}: At a glance, the results for MS_{AP} (Fig. 8a) raise doubt on the correctness of the previous results and the basic assumption. Considering the longitudinal MSs of the first log (SANDED L1, ROUGH L1) the expected increase is interrupted for both subsets. This interrupt is also shown for the second log (SANDED L2, ROUGH L2) for the SDGs 14, 15. Interestingly, these interrupts can be recognized for MS_F and the fusion procedure $MS_{AP,F}$ too.

A closer examination of the CS-Slices of L1, L2 and L3 provides an answer for the differing results. For L3 just the CS-Slices at the log ends show up knots. Hence, for larger distances the longitudinal MSs (MS_{AP}) increase additionally and the expected trend becomes strengthened. In contrast to L3, L1 and L2 show up knotty
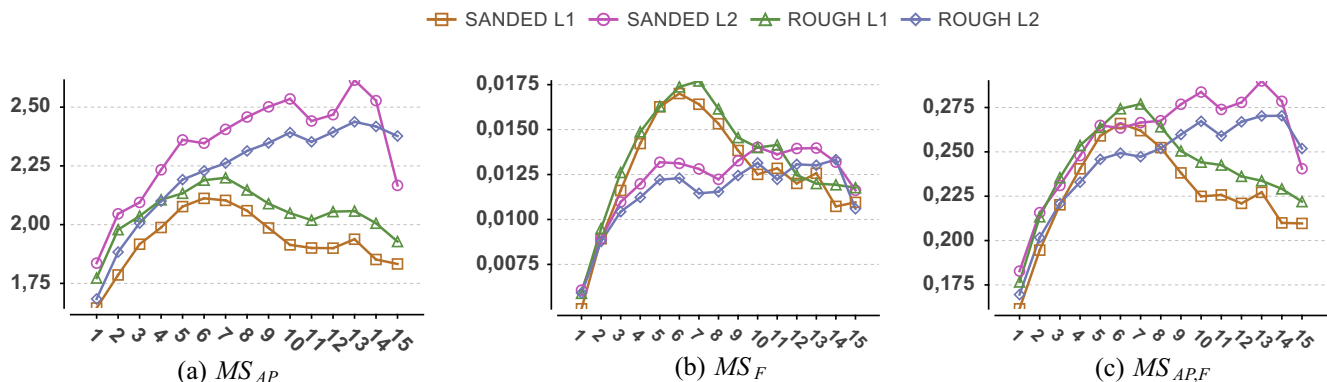

Fig. 8. Intraclass SD: Rough and Sanded longitudinal MSs of L1 and L2 grouped by the slice distance. [*X*-Axis: Slice Distance Group, *Y*-Axis: Matching Score].
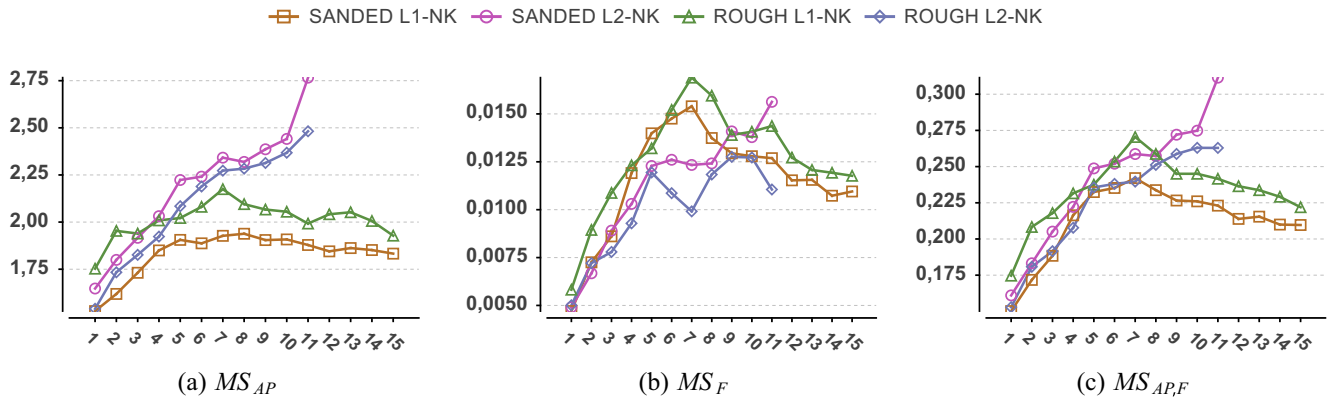
Fig. 9. Longitudinal variance analysis excluding knotty CS-Slices – L1(#9, 10, 14), L2(#1, 2, 10, 11, 15, 16). [*X*-Axis: Slice Distance Group, *Y*-Axis: Matching Score].
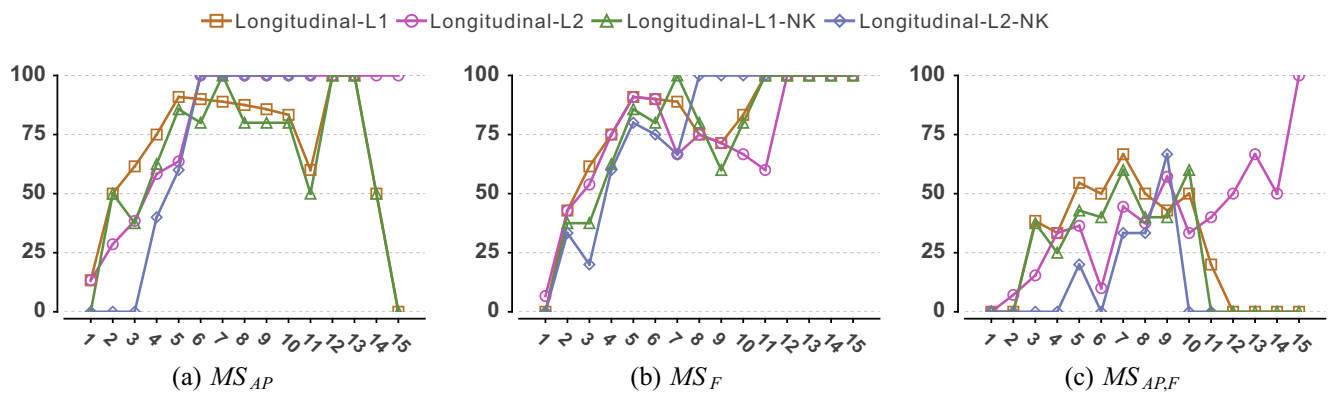

Fig. 10. Interclass fractions for the slice distance groups (SDGs) of each longitudinal SD subset. [*X*-Axis: Slice Distance Group, *Y*-Axis: Interclass Fraction (%)].

CS-Slices situated in the middle of each log. For L1 three (#9, 10, 14 – see Fig. 4d) and for L2 six CS-Slices (#1, 2, 10, 11, 15, 16) show up between one and four knots. By omitting MSs from those knotty CS-Slices the results in Fig. 9 approximately show the expected trend. Quite interesting is the good MS at SDG 15 for SANDED L2 (MS_{AP}) which results from one equally located knot in the CS-Slices #1 and #16.

This leads to two major conclusions: Less surprising, the results demonstrate that MSs between non-knotty (NK) and knotty CS-Slices are remarkably worse. Second, the results indicate that knots do not introduce any propagative effects to the annual ring pattern and the CS shape.

In comparing the results from L1 to L2 it is visible that the ranges of the longitudinal MSs for different logs vary. Figs. 8 and 9 illustrate that the MSs of L2 are worse compared to L1, especially when considering larger slice distances. However, it can be stated that the longitudinal MSs of each log are getting worse with an increasing slice distance.

Longitudinal SD/interclass fractions. The longitudinal increase of the MSs leads to the conjecture that for higher slice distances it is not possible to separate between longitudinal MSs and interclass MSs. This conjecture is validated by considering the interclass fraction of the MSs of all SDGs for each longitudinal SD subset. The interclass fraction of a SDG is specified as the percentage of MSs (within a longitudinal SD subset and SDG) which intersect with the interclass SD. The interclass fractions of each longitudinal SD subset and SDG are illustrated in Fig. 10. For MS_{AP} and MS_F the results confirm the expectation that for larger slice distances the fraction of MSs which intersects with the interclass SD increases. The differences between the knot-including and knot-free SDs

are not significant. Just for the Longitudinal-L2-NK SD and MS_{AP} the fractions of the first three SDGs (1–3) are pushed down to zero.

Most important, the results for $MS_{AP,F}$ illustrate that by the fusion of pattern and shape information the interclass fractions decrease for all subsets. The robustness to longitudinal variations is improved significantly by feature fusion.

3.2.2. Surface SD

The surface SD is examined in context of the previously analysed longitudinal SD subsets and the interclass SD. Again, the main objective is to assess the separability between the surface SD subsets and the interclass SD. In case of the CS-Images of L1 and L2 the surface MSs are the only MSs between CS-Images from equal CS-Slices in our experiments. The surface MSs between the rough and sanded CS-Images are considered for L1 and L2, separately. For all SDs the cumulative distribution functions (CDF) are computed and illustrated for each matching procedure (see Fig. 11). The CDF of a SD gives the probability that a certain MS exists that is ranged less or equal to that MS. Furthermore, the CDF illustrates the median value at a probability of 0.5 – half of the MSs are lower and half of the MSs are higher than the median. The CDFs of a certain intraclass SD group/subset and the interclass SD are used to observe their overlap and to draw conclusions about their separability.

Generally, it is expected that the surface SD subsets consist of very good MSs and their CDFs are thus aligned in front (=left hand side) of the longitudinal SD CDFs. For all surface SD subsets and matching procedures no overlaps with the interclass CDF are shown. For MS_F the surface SD subsets show very good MSs because the shape difference between the rough and sanded
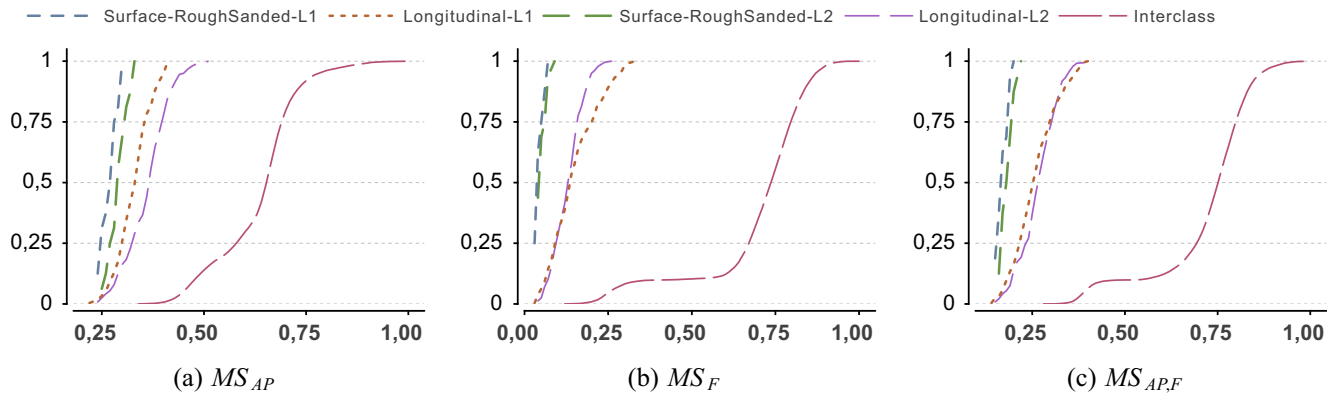
Fig. 11. Cumulative distribution functions (CDFs) for different longitudinal and surface SD subsets and the interclass SD. [*X*-Axis: Matching Score, *Y*-Axis: Probability].

CS-Image of a CS-Slice is very low. The overlaps between the longitudinal SDs and the interclass SD have been discussed in the previous section. Again, the results for $MS_{AP,F}$ show that fusion improves the separability between the longitudinal SD subsets and the interclass SD.

3.3. Identification performance

So far, all evaluations were related to the verification performance of log end biometrics. Based on the gathered insights, two investigations on the identification performance are presented: First, the MSs for each CS-Slice of L1 and L2 are ordered and the ranks for different intraclass MS groups/subsets and the interclass MSs are analysed. Hence, general statements on the rank orders can be presented.

Second, the identification rates for four specific identification scenarios are presented. All scenarios illustrate the impact of cutting the log end on the identification performance. As such, it is elaborated how the width of the piece which is cut-off influences the performance. Additionally, the impact of using different cutting tools is assessed.

3.3.1. Cumulative CS-Slice matching score ranks

Commonly, the CMC depicts how the biometric system ranks the MSs between a set of probe templates and all database templates. The CMC curve illustrates the probability that the correct (intraclass) MS is ranked within the first *k*-ranks. In case of 100% identification rate the CMC curve shows a detection rate of 100% at the first rank. For this investigation, the SD-MS rankings of five different intraclass groups/subsets and the first observation of an interclass SD-MS are assessed.

For each CS-Slice the MSs between each of its templates and all other templates in the database are ordered in an ascending order. In Fig. 12 the detection rates for four SD groups/subsets and the interclass SD are depicted:

– SURFACE: Detection rate for the MSs between the rough and sanded CS-Images of each CS-Slice.
– ROUGH-LONG, SANDED-LONG for L1 & L2: Detection rates for longitudinal MSs from slice distance group 1 or 2. These are of interest in an industrial application (e.g. cutting the log end once or twice).
– INTER: Detection rate for observing the first interclass MS.

For example, in Fig. 12a the SURFACE curve shows that there is ∼30% chance of finding the corresponding rough or sanded surface as the best match and ∼95% chance to find it among the top 10 ranked matches. The INTER curve shows that there is 0% risk of finding a CS-Slice from another log as the best match but ∼5% risk of finding a CS-Slice from another log among the top 20 ranked matches.

Based on the CMC curves we can draw interesting conclusions on the identification performance of the biometric system. Most important, for all matching procedures and CS-Slices each considered intraclass SD group/subset shows up high detection rates at the best (=lowest) ranks. On the other hand, the probability of observing a well ranked (<15) interclass SD-MS is nearly zero. In case of $MS_{AP,F}$ nearly all intraclass SD-MSs are ranked in front of the first interclass SD-MS occurrence. Notice that a larger amount of different logs in the testset could have a big impact on the results.

In comparing the surface SD ranks to the longitudinal SD subset ranks the results lead to an interesting observation. The MSs (MS_{AP}) of the rough and sanded longitudinal SDs of L1 and L2 are ranked in the range of the surface SD-MSs. Thus the results distinguish from
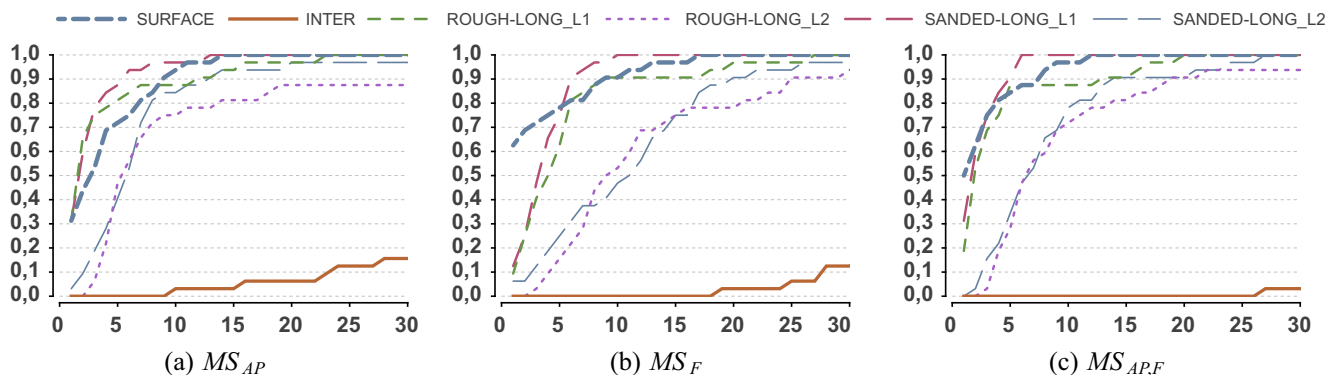

Fig. 12. Cumulative matching score ranks. [*X*-Axis: Rank, *Y*-Axis: Detection Rate].

the verification performance results in Fig. 11 where the surface CDFs show better MSs than the longitudinal CDFs. This illustrates that CS-Images of adjacent neighboured CS-Slices with the same kind of surface show up a high annual ring pattern similarity to each other. Because of longitudinal shape variations the results for MS_F show that the longitudinal MSs are ranked worse compared to the SURFACE MSs.

Again, the results depict a higher longitudinal CS variability of L2 which is demonstrated by the higher ranked (=worse) MSs for the longitudinal SD subsets of L2.

Concluding, the results show that the first occurrence of an interclass MS is worse ranked (=higher ranked) compared to the intraclass MSs. The interclass CMC curves for $MS_{AP,F}$ show that for feature fusion the interclass detection rates shift remarkably to higher ranks.

3.3.2. Identification performance – test scenarios

Finally, the identification performance for different scenarios is assessed. A test scenario requires to specify a probe set and a gallery set. The gallery specifies the enrolled templates of the individuals/objects contained in the database. The probe set is a set of templates of individuals/objects which are used to query the biometric system. For each probe template the matches/MSs to all database templates are computed. The computed matches/MSs for each probe template are ordered and the rank of the correct match/MS is determined. Subsequently, for each rank the probability that the correct match/MS is equal or better ranked is computed. For illustration these probabilities are depicted in a CMC chart. The probability that the correct match is ranked at the first position is denoted as identification rate or detection rate. Basically, all scenarios evaluate the impact of cutting the log end in the sawmill.

Scenario #1, #2 – same cutting tool. For these scenarios it is assumed that the first cut in the forest and the second cut in the sawmill is performed with the same cutting tool. Hence, no surface variations due to different cutting tools are introduced. For this purpose Scenario #1 (Rough-Rough) is based on rough CS-Images and Scenario#2 (Sanded-Sanded) is based on sanded CS-Images of L1 and L2. As probe templates for Scenario#1, #2 the rough or sanded CS-Images of each CS-Slice are utilized, respectively.

For each scenario and probe template it is assumed that just one equally surfaced CS-Image of the same log which belongs to a certain slice distance group (SDG) is enrolled in the gallery set. For evaluation the SDGs 1–5 are considered. Furthermore, templates of all CS-Images from L3 and equally surfaced CS-Images of the other log (L1 or L2) are included in the gallery. For each probe template the rank of the correct match is computed and in Table 4 the results for both scenarios are summarized. For each scenario the identification rates for different SDGs and matching procedures are illustrated.

The results for Scenario#1 and #2 in Table 4 show high detection rates for the first four SDGs. The results illustrate that for SDG 4 and 5 the detection rates of MS_F decrease to a higher degree than for MS_{AP}. Basically, it is recognizable that the identification rates for both scenarios and matching procedures are somewhat equal. Consequently, the CS shape has less impact on the identification performance of Scenario#1 and #2. For $MS_{AP,F}$ and the SDGs 1, 2 the identification rates account 100% for both scenarios. These results are a first indication that log end biometrics are probably robust to cutting the log end in a range of five centimetres (2 CS-Slices = 5 cm). In case of $MS_{AP,F}$ the rates for higher SDGs are still in a range between 84% and 97%. In Fig. 13 the CMC curves for $MS_{AP,F}$ and both scenarios are illustrated.

Scenario #3, #4 – different cutting tools. In difference to the first two scenarios, Scenario #3 and #4 investigate the impact of different surfaced CSs. Thus, it is assumed that the first cut in the forest and the second cut in the sawmill are performed with different cutting tools. Based on the CS-Images of L1 and L2 two scenarios are constructed. Scenario #3 (Rough-Sanded) assumes that the first cut is represented by a rough CS-Image of a CS-Slice and the second cut is represented by a sanded CS-Image of a neighboured CS-Slice. Scenario #4 (Sanded-Rough) assumes that the cuts are performed in the reverse order. Consequently, these scenarios simulate a mixture of longitudinal and surface CS variations. For both scenarios the rank-orders for the correct matches are computed in the same way as for the first two scenarios (see Table 5). The results for Scenario #3 in Table 5 illustrate that for all matching procedures the identification performance decreases for higher SDGs. Compared to Scenario#1 and #2, the identification rates for MS_{AP} are worse. This is caused by the CS surface variations which cause a decrease of the identification performance for MS_{AP}. Nevertheless, the results for $MS_{AP,F}$ are convincing and for SDG 1, 2 an error free identification performance is achieved (Fig. 13).

Finally, the results for all scenarios indicate that log end biometrics are robust to longitudinal variations and mixtures of surface and longitudinal variations to a certain degree. Furthermore, and equal as in Schraml et al. (2015a) all evaluations showed that the fusion of annual ring pattern and shape information is valuable to increase the performance of the biometric system.

Table 4
Scenario#1, #2 – Identification rates for different slice distance groups (SDGs) and matching procedures (MPs).

MP/SDG	1	2	3	4	5
#1 Rough-Rough					
MS_{AP}	1.0	1.0	0.97	0.97	0.91
MS_F	1.0	0.94	0.91	0.84	0.78
$MS_{AP,F}$	1.0	0.97	0.91	0.81	0.75
#2 Sanded-Sanded					
MS_{AP}	1.0	0.97	0.94	0.91	0.69
MS_F	1.0	0.94	0.91	0.88	0.66
$MS_{AP,F}$	1.0	1.0	0.94	0.81	0.66

(a) #1 Rough-Rough   (b) #2 Sanded-Sanded   (c) #3 Rough-Sanded   (d) #4 Sanded-Rough
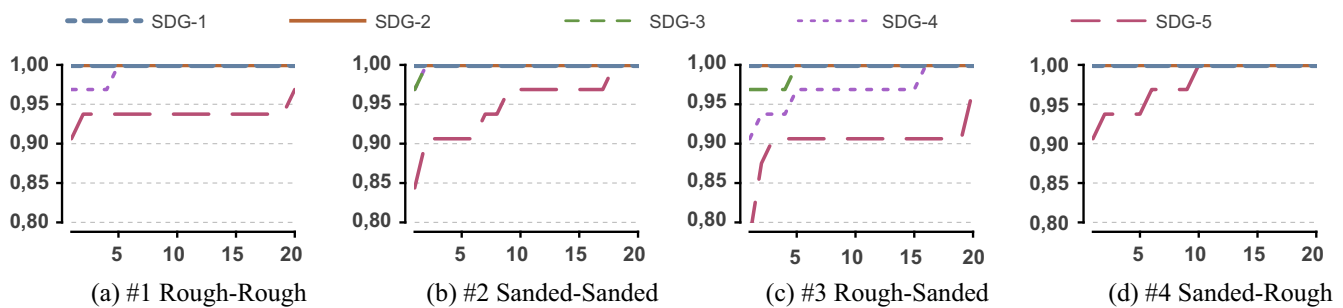
Fig. 13. $MS_{AP,F}$: CMC curves for the different scenarios and slice distance groups. [*X*-Axis: Rank, *Y*-Axis: Detection Rate].

Table 5
Scenario#3, #4 – Identification rates for different slice distance groups (SDGs) and matching procedures (MPs).

MP/SDG	1	2	3	4	5
#3 Rough-Sanded					
MS_{AP}	0.97	0.91	0.91	0.72	0.69
MS_F	0.94	0.88	0.91	0.63	0.56
$MS_{AP,F}$	1.0	0.94	0.91	0.81	0.66
#4 Sanded-Rough					
MS_{AP}	0.94	0.88	0.84	0.78	0.69
MS_F	0.91	0.81	0.84	0.66	0.56
$MS_{AP,F}$	1.0	1.0	0.97	0.81	0.78

4. Conclusions

The findings of this study show that log end biometrics are promising to discriminate between different tree logs in an industrial application. It can be concluded that the robustness of the biometric system to CS variations depends to a high degree on the template computation approach and the matching procedure.

In comparing the results for three different matching procedures it is obvious that biometric feature fusion increases the robustness significantly. In regard to the verification performance, a combination of annual ring pattern and shape features increases the robustness to longitudinal CS variations. Furthermore, the analysis of the intraclass SD groups illustrates that CS surface variations are not crucial for the verification performance.

Based on the identification performance experiments we conclude that biometric log recognition is qualified to overcome the issue of cutting log ends in the sawmill. Results show a successful identification within cutting off slices up to ~5 centimetres in thickness, even if the second cut in the sawmill is performed with another cutting tool.

The analysis of the longitudinal CS variations for different SDGs shows that knots are disturbing factors. This is caused by the fact that the current approach is not dealing with knots on CSs. Surprisingly, the results indicate that knots do not introduce any propagative effects to the annual ring pattern and the CS shape. Thus, future work should investigate the similarity between non-knotty parts of knotty CSs and their neighboured knot free CSs.

5. Future work

Although the results of this study together with the results in Schraml et al. (2015a,b) are very promising, further experiments on a large set of tree logs are indispensable to assess the identification performance in a real world environment. Furthermore, future work has to deal with the impact of typical external CS surface variations which are caused by dirt, snow or ice during transportation or storage. Regarding log template computation and matching, the applicability of other feature extraction methods should be assessed and new approaches should be developed. Finally, further research should deal with the impact of automatic pith estimation and CS segmentation approaches to the biometric system performance.

References

Barrett, W., 2008. Biometrics of cut tree faces. In: Sobh, T. (Ed.), Advances in Computer and Information Sciences and Engineering. Springer, Netherlands, pp. 562–565.

Chiorescu, S., Grönlund, A., 2003. The fingerprint approach: using data generated by a 2-axis log scanner to accomplish traceability in the sawmill's log yard. For Prod J 53, 78–86.

Chiorescu, S., Grönlund, A., 2004. The fingerprint method: using over-bark and under-bark log measurement data generated by three-dimensional log scanners in combination with radiofrequency identification tags to achieve traceability in the log yard at the sawmill. Scand. J. For. Res. 19, 374–383.

Dykstra, D.P., Kuru, G., Taylor, R., Nussbaum, R., Magrath, W.B., Story, J., 2003. Technologies for Wood Tracking. Technical Report. World Bank – WWF Alliance Report.

EuropeanParliament, 2010. Regulation (EU) No 995/2010 of the European Parliament and of the Council of 20th October 2010 Laying Down the Obligations of Operators who Place Timber and Timber Products on the Market.

Flodin, J., Oja, J., Grönlund, A., 2007. Fingerprint traceability of sawn products using X-ray log scanning and sawn timber surface scanning. In: Proceedings of Quality Control for Wood and Wood Products: COST Action E 53 the First Conference.

Flodin, J., Oja, J., Grönlund, A., 2008a. Fingerprint traceability of logs using the outer shape and the tracheid effect. For. Prod. J. 58, 21–27.

Flodin, J., Oja, J., Grönlund, J., 2008b. Fingerprint traceability of sawn products using industrial measurement systems for X-ray log scanning and sawn timber surface scanning. For. Prod. J. 58, 11.

Hong, L., Wan, Y., Jain, A., 1998. Fingerprint image enhancement: algorithm and performance evaluation. IEEE Trans. Pattern Anal. Mach. Intell. 20, 777–789.

Jain, A., Ross, A., Prabhakar, S., 2001. Fingerprint matching using minutiae and texture features. In: Proc. of the International Conference on Image Processing (ICIP'01), Thessaloniki, GR. pp. 282–285.

Jain, A.K., Flynn, P., Ross, A.A., 2007. Handbook of Biometrics. Springer, New York, USA.

Jain, A.K., Prabhakar, S., Hong, L., Pankanti, S., 2000. Filterbank-based fingerprint matching. IEEE Trans. Image Process. 9, 846–859.

Jain, A.K., Ross, A.A., Nandakumar, K., 2011. Introduction to Biometrics. Springer, US.

Kastner, T., Erb, K.H., Nonhebel, S., 2011. International wood trade and forest change: a global analysis. Glob. Environ. Change 21, 947–956.

Knutsson, H., Granlund, G.H., 1983. Texture analysis using two-dimensional quadrature filters. In: IEEE Computer Society Workshop on Computer Architecture for Pattern Analysis and Image Database Management, Pasadena, USA.

Kuemmerle, T., Chaskovskyy, O., Knorn, J., Radeloff, V.C., Kruhlov, I., Keeton, W.S., Hostert, P., 2009. Forest cover change and illegal logging in the ukrainian carpathians in the transition period from 1988 to 2007. Remote Sens. Environ. 113, 1194–1207.

Maltoni, D., Maio, D., Jain, A.K., Prabhakar, S., 2009. Handbook of Fingerprint Recognition. Springer, New York, USA.

Marjanen, K., Ojala, P., Ihalainen, H., 2008. Measurement of annual ring width of log ends in forest machinery. In: Proceedings of the SPIE Conference on Image Processing: Algorithms and Systems.

Mattila, P., Viittanen, J., 1999. Method and Measuring Apparatus used in Conjunction with a Tree-working Device.

Norell, K., 2009. An automatic method for counting annual rings in noisy sawmill images. In: Proceedings of the Conference on Image Analysis and Processing (ICIAP). Springer, Berlin/Heidelberg, pp. 307–316.

Norell, K., Borgefors, G., 2008. Estimation of pith position in untreated log ends in sawmill environments. Comput. Electron. Agric. 63, 155–167.

Pahlberg, T., Hagman, O., Thurley, M., 2015. Recognition of boards using wood fingerprints based on a fusion of feature detection methods. Comput. Electron. Agric. 111, 164–173.

Richards, M., Wells, A., Del Gatto, F., Contreras-Hermosilla, A., Pommier, D., 2003. Impacts of illegality and barriers to legality: a diagnostic analysis of illegal logging in Honduras and Nicaragua. Int. For. Rev. 5, 282–292.

Schraml, R., Charwat-Pessler, J., Uhl, A., 2014. Temporal and longitudinal variances in wood log cross-section image analysis. In: IEEE International Conference on Image Processing 2014 (ICIP'14), Paris, FR. pp. 5706–5710.

Schraml, R., Hofbauer, H., Petutschnigg, A., Uhl, A., 2015a. Tree log identification based on digital cross-section images of log ends using fingerprint and iris recognition methods. In: Proceedings of the 16th International Conference on Computer Analysis of Images and Patterns (CAIP'15). Springer, Valetta, MT, pp. 752–764.

Schraml, R., Petutschnigg, A., Uhl, A., 2015b. Validation and reliability of the discriminative power of geometric wood log end features. In: Proceedings of the IEEE International Conference on Image Processing (ICIP'15), Quebec, CAN.

Schraml, R., Uhl, A., 2013. Pith estimation on rough log end images using local fourier spectrum analysis. In: Proceedings of the 14th Conference on Computer Graphics and Imaging (CGIM'13), Innsbruck, AUT.

Schraml, R., Uhl, A., 2014. Similarity based cross-section segmentation in rough log end images. In: Iliadis, L., et al. (Eds.), Proceedings of the 10th Artificial Intelligence Applications and Innovations Conference (AIAI'14), Rhodes, GR. pp. 614–621.

Smith, J., Obidzinski, K., Subarudi, S., Suramenggala, I., 2003. Illegal logging, collusive corruption and fragmented governments in Kalimantan, Indonesia. Int. For. Rev. 5, 293–302.

Tzoulis, I., Andreopoulou, Z., 2013. Emerging traceability technologies as a tool for quality wood trade. Procedia Technol. 8, 606–611.

United Nations, 1992. United Nations Conference on Environment & Development. Agenda 21, Rio de Janeiro, BR.